Metal–Ligand Vibrations of Cyanoferric Myeloperoxidase and Cyanoferric Horseradish Peroxidase: Evidence for a Constrained Heme Pocket in Myeloperoxidase†

Juan J. Lôpez-Garriga,‡,§ W. Anthony Oertling,‡,∥ Robert T. Kean,‡,⊥ Hans Hoogland,#,○ Ron Wever,# and Gerald T. Babcock*,‡

Department of Chemistry and the LASER Laboratory, Michigan State University, East Lansing, Michigan 48824, and E. C. Slater Institute for Biochemical Research, University of Amsterdam, Plantage Muidergracht 12, 1018 TV Amsterdam, The Netherlands

Received April 4, 1990; Revised Manuscript Received July 2, 1990

ABSTRACT: The low-frequency FeCN vibrations of cyanoferric myeloperoxidase (MPO) and horseradish peroxidase (HRP) have been measured by resonance Raman spectroscopy. The ordering of the frequencies of the predominantly FeC stretching and FeCN bending normal vibrational modes in the two peroxidases differs. These normal mode vibrations are identified by their wavenumber shifts upon isotopic substitution of the cyanide ligand. For MPO, the stretching mode ν_1 (361 cm^{-1}) occurs at a lower frequency than the bending mode δ_2 (454 cm^{-1}). For HRP, the order is reversed as ν_1 (456 cm^{-1}) is at a higher frequency than δ_2 (404 cm^{-1}). Normal coordinate analyses and model complexes have been used to address the origin of this behavior. The ν_1 stretching frequencies in cyanide complexes of iron porphyrin and iron chlorin model compounds are similar to one another and to that of HRP. Thus, the inverted order and altered frequencies of the ν_1 and δ_2 vibrations in MPO, relative to those in HRP and the model compounds, are not inherent to the proposed iron chlorin prosthetic group in MPO but, rather, are attributed to distinct distal environmental effects in the MPO active site. The normal coordinate analyses for MPO and HRP showed that the ν_1 and δ_2 vibrational frequencies are not pure; the potential energy distributions for these modes respond not only to the geometry but also to the force constants of the ν(FeC) and δ(FeCN) internal coordinates. By assuming a bent structure of the FeCN moiety in MPO relative to that in HRP, we were able to reproduce the reversed order of the ν_1 and δ_2 frequencies in the leucocyte enzyme. The pH dependence of the Raman spectrum of cyanide-bound MPO supports the occurrence of a bent axial ligand structure. We invoke both distal and proximal effects to explain the FeCN vibrations of MPO. The amino acid residues responsible are judged to be those relevant to the catalytic properties of the enzymes.

Myeloperoxidase (MPO), an enzyme found in leukocytes in blood plasma, is an integral component of the antimicrobial response, owing to its ability to catalyze the formation of HOCl from Cl^- and H_2O_2. The active site of the enzyme contains an iron chromophore with optical properties superficially similar to those of heme proteins. However, the details of the MPO absorption spectra, particularly its red-shifted Soret band (Wever & Plat, 1981), and of its resonance Raman spectra (Sibbett & Hurst, 1984; Babcock et al., 1985) are significantly different from those of the peroxidase enzymes that contain a protoheme IX chromophore (Rakhit & Spiro, 1974; Kimura et al., 1981; Desbois et al., 1984; Sibbett et al., 1985; Manthey et al., 1986, Andersson et al., 1985, 1987; Smulevich et al., 1988). This peculiar behavior suggests that the prosthetic group of myeloperoxidase (MPO) has a unique structure and possibly a unique apoprotein environment. Both chlorin-type (Morell et al., 1967; Eglington et al., 1982; Sibbett & Hurst, 1984; Babcock et al., 1985, Ikeda-Saito et al., 1985; Stump et al., 1987) and heme *a* type (Schultz et al., 1964, Newton et al., 1965; Bakkenist, 1981) structures have been suggested for the MPO chromophore. Although the chlorin proposal is now favored by most of the workers in the field, neither a chlorin nor a heme *a* origin is sufficient to explain all of the spectroscopic properties of the enzyme.

The details of the MPO catalytic cycle have been studied, and the key steps in this process have been identified. Upon reaction with hydrogen peroxide, MPO forms an intermediate (MPO compound I) which catalyzes the oxidation of chloride ion to hypochlorous acid (Agner, 1970; Stelmaszynska et al., 1974; Harrison et al., 1976; Klebanoff et al., 1978). Upon further reaction with hydrogen peroxide, MPO compound I may form another intermediate (MPO compound II), which shows a pH-dependent absorption spectrum (Hoogland et al., 1987). Oertling et al. (1988) used resonance Raman spectroscopy to establish that MPO forms an oxoferryl ($O = Fe^{IV}$) derivative with its iron–oxygen stretching frequency at 782 cm^{-1}. This vibrational frequency is similar to that reported for the oxoferryl intermediates of horseradish peroxidase (HRP) (Hashimoto et al., 1984; Terner et al., 1985; Makino et al., 1986; Oertling & Babcock, 1988) and suggests that in

† This study was supported by grants from the Netherlands Organization for the Advancement of Pure Research (Z.W.O.) under the auspices of the Netherlands Foundation for Chemical Research (S.O.N.) to R.W. and from the U.S. National Institutes of Health (GM 25480) to G.T.B. J.J.L.-G. acknowledges the receipt of the Provost Affirmative Action Postdoctoral Fellowship from Michigan State University. This collaboration was made possible by a NATO Research Grant (86/734).

‡ Michigan State University.

§ Present address: Department of Chemistry, University of Puerto Rico, Mayaguez, Mayaguez, PR 00708.

∥ Present address: Inorganic and Structural Chemistry Group, INC-4 Mail Stop C-345, Los Alamos National Laboratory, Los Alamos, NM 87545.

⊥ Present address: Cargill Inc., Research Division, P.O. Box 9300, Minneapolis, MN 55440.

University of Amsterdam.

○ Present address: State Institute for Quality Control of Agricultural Products, Bornsesteeg 45, 6708 PD Wageningen, The Netherlands.

0006-2960/90/0429-9387$02.50/0

both peroxidases the heme protein pocket imposes similar structural configurations, at least for monoatomic ligands.

When a bulkier distal ligand is employed, however, the axial ligand–metal interactions in MPO and HRP may differ. Thus, this class of ligand may provide more incisive information as to the nature of the catalytic constraints imposed by the active sites in these two peroxidases. To assess this possibility, we carried out resonance Raman (RR) measurements of the Fe^{3+}–CN^- vibrations of HRP and MPO. The behavior of the iron–cyanide vibrations in the two enzymes differs significantly. In fact, the ordering of the frequencies that display isotopic shifts characteristic of the stretching and bending normal modes is inverted in MPO relative to that in HRP. Model compound and normal coordinate analyses suggest that these effects result from the occurrence of a more constrained distal pocket in MPO which forces a bent FeCN geometry. Recent Raman data obtained by Han et al. (1989) indicate that similar steric constraints occur in the cyanide binding site in ferric sulfite reductase. Our analysis indicates that the protein groups that modify the axial ligand–iron vibrations in the peroxidases are most likely those involved in the catalytic reactions of oxoferryl intermediates (Dunford, 1982; Bolscher & Wever, 1984).

Experimental Procedures

Sample Preparations. MPO was purified from human leukocytes, according to the procedure of Bakkenist et al. (1978). Its concentration was determined by using an absorbance coefficient of 89 mM^{-1} cm^{-1} per heme at 428 nm (Agner, 1958). The ratio A_{428nm}/A_{280nm} for the preparation was 0.8 or higher. HRP was purchased from Sigma (type VI) and used without further purification. Its concentration was measured by using an absorbance coefficient at 403 nm of 103 mM^{-1} cm^{-1} (Schonbaum & Lo, 1972). $Na^{13}C^{14}N$, $Na^{13}C^{15}N$, and $K^{12}C^{15}N$ (99%) were purchased from Cambridge Isotopes Laboratories and MSD Isotopes. $Na^{12}C^{14}N$ was from J. T. Baker Chemical Co. The integrity of the $Na^{12}C^{14}N$, $Na^{13}C^{14}N$, and $K^{12}C^{15}N$ reagents was confirmed by Raman measurements on 10 mM stock solutions (pH 11), which yielded C≡N stretching frequencies of 2080, 2037, and 2048 cm^{-1}, respectively, in agreement with Yoshikawa et al. (1985). Cyanide binding to heme iron was achieved by adding aliquots of these stock solutions to native ferric enzyme samples in either 100 mM phosphate buffer for neutral pH experiments or 100–400 mM carbonate buffer for alkaline pH measurements. The specific pH values and other conditions are given in the figure legends.

Chloride salts of ferric deuteroporphyrin dimethyl ester and ferric deuterochlorin were supplied by Professor C. K. Chang, Michigan State University. The dimethyl ester of ferric deuterochlorin was prepared by refluxing with trifluoroacetic anhydride under nitrogen in a methylene chloride/methanol mixture (Wang et al., 1958). Bis-cyanide complexes were prepared by using the following procedure. Approximately 61 μmol of solid KCN was dissolved in 1 mL of a buffered detergent solution [0.1 M phosphate, pH 8.4, 0.2% (w/v) Brij 35 (Sigma)] to produce a final pH of 10.7. The chloride salt of iron(III) porphyrin or chlorin was dissolved in methylene chloride and vortexed with the cyanide solution under a stream of argon. As the methylene chloride evaporated, transfer of the iron complex to the aqueous solution resulted. The mono(1-methylimidazole), monocyanide complexes were prepared by addition of 1-methylimidazole to the bis-cyanide complexes; the displacement of one of the CN^- ligands by the 1-methylimidazole was observed in the optical spectrum and confirmed by resonance Raman spectroscopy (Kean, 1987).

Raman Measurements. Samples of proteins for Raman measurements were contained (0.8-mL volume) in a cylindrical, quartz, spinning cell that was maintained at 5–10 °C by flowing cold nitrogen gas. Sample integrity was confirmed by optical absorption and pH measurements before and after laser irradiation. Additional details appear in the figure captions. Raman spectra were obtained by using a computer-interfaced Spex 1401 Ramalog spectrometer in conjunction with Spectra Physics Model 164 argon (457.9 mn) and Model 165 krypton (406.7 nm) ion lasers and a Coherent Innova 90 krypton (413.1 nm) ion laser.

Vibrational Analyses. Vibrational analyses were carried out for a simplified model system that consisted of imidazole–Fe–CN. The porphyrin system was represented by four equally-distributed point masses (104 amu), situated in the position of the pyrrole nitrogens. Imidazole was treated as a single unit with a mass of 68 amu. As Yu et al. (1984) indicated for a linear geometry with the ligand perpendicular to the ring, no differences were found between the FeC stretching ν_1 or FeCN bending δ_2 normal mode frequencies when they were calculated by this approach and when they were calculated by neglecting the porphyrin ring altogether. However, we found that, when the FeCN angle is reduced to 155°, neglecting the porphyrin ring influences the ν_1 stretching and δ_2 bending frequencies and the potential energy distributions (PED) of these modes slightly (<5%).

The Shimanouchi (1969) normal coordinate analysis program was used for the calculations. The geometry and force field of transition-metal cyanide complexes (Swanson, 1976; Jones et al., 1974; Swanson & Rafalko, 1976), as well as the crystal structures of cyanoferric erythrocruorin (Steigemann & Weber, 1979) and cyanometalloporphyrin complexes (Scheidt et al., 1980, 1983), were employed to construct the geometry and initial force field for the normal mode calculations. The following bond lengths (Å) were used: ImFe = 2.025, FeC = 1.908, CN = 1.152, and FeN_p = 1.970. The Im–Fe–C moiety was assumed linear and perpendicular to the porphyrin plane. The FeCN bond angle [θ (deg)] was then varied in order to give the best fit for the MPO–CN and HRP–CN cases, as discussed below. These calculations were performed within the constraints imposed by the X-ray studies of cyanoferric yeast cytochrome *c* peroxidase (Poulos et al., 1978) and cyanoferric erythrocruorin (Steigemann & Weber, 1979), which show FeCN angles of 130° and 164°, respectively.

The initial force field employed for the diagonal terms was as follows: S(CN) = 16.9, S(FeC) = 1.85, S(ImFe) = 1.461, S(FeNp) = 1.0, B(FeCN) = 0.5, and B(ImFeC) = 0.40 (in-plane and out-plane motions). For the off-diagonal terms, the following values were used: S/S(ImFe/CN) = 0.218, S/S-(FeC/CN) = 0.34, and S/B(FeC/FeCN) = 0.2. The units used for these force constants were mdyn/Å for the stretching (S) and the stretch/stretch interaction (S/S) force constants, mdyn/rad for the stretch/bend (S/B) interaction force constants, and mdyn Å/rad^2 for the bending (B) force constants. In order to constrain the off-diagonal force constants in our MPO and HRP vibrational analysis, we carried out a perturbative study of the effect of these force constants on the ligand vibrations in the insect cyanometHb CTT III system (Yu et al., 1984), where the ν_1 and δ_2 frequencies and isotopic frequencies are well-defined. With the above data, and assuming an FeCN angle of 170° (Yu et al., 1984), we fit the isotopic frequencies of cyanometHb CTT III. The results showed that the ν_1 stretching and δ_2 bending frequencies (453 cm^{-1} and 412 cm^{-1}, respectively) are practically independent

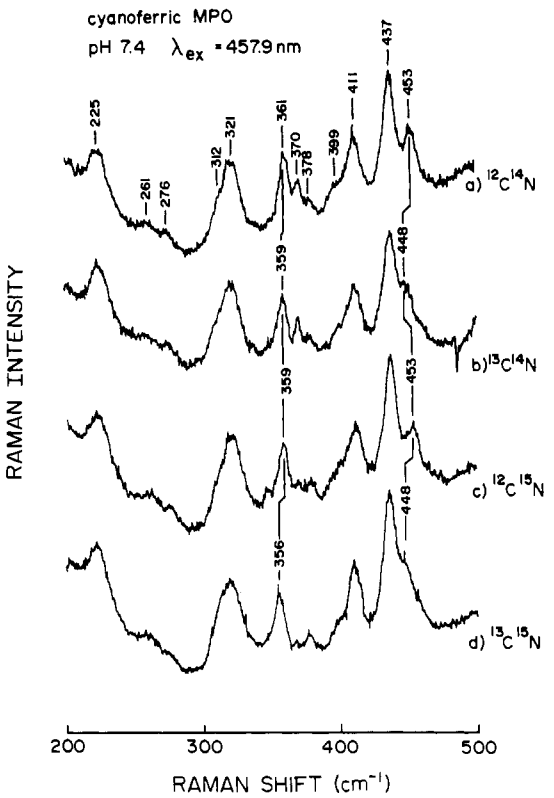

FIGURE 1: Low-frequency resonance Raman spectra of isotopically labeled cyanoferric MPO. Conditions: [enzyme chromophore] = 0.025 mM; [total cyanide] = 0.4 mM in 100 mM phosphate buffer; sample pH 7.4; λ_{ex} = 457.9 nm; laser power 40 mW; total of three to five scans per spectrum. (a) $^{12}C^{14}N$, (b) $^{13}C^{14}N$, (c) $^{12}C^{15}N$, and (d) $^{13}C^{15}N$. The feature at 370 cm^{-1} is from a small amount of native enzyme not bound by cyanide.

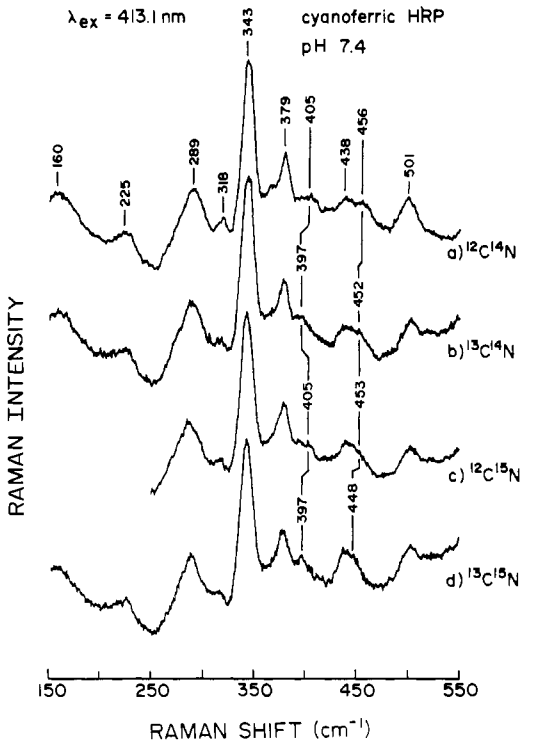

FIGURE 2: Low-frequency resonance Raman spectra of isotopically labeled cyanoferric HRP. Conditions: [enzyme chromophore] = 0.05 mM; [total cyanide] = 0.75 mM in 100 mM phosphate buffer; sample pH 7.4; λ_{ex} = 413.1 nm; laser power 30 mW; total of eight to nine scans per spectrum. (a) $^{12}C^{14}N$, (b) $^{13}C^{14}N$, (c) $^{12}C^{15}N$, and (d) $^{13}C^{15}N$.

of the S/S(ImFe/CN) and S/S(FeC/CN) interaction force constants. In the case of the S/B(FeC/FeCN) interaction force constant, however, we noticed a small dependence of the numerical vibrational frequencies and, more importantly, a significant shift of potential energy distribution (PED). This may be expected because internal coordinates [in this case, ν(FeC) stretch and δ(FeCN) bend coordinates] with similar natural frequencies interact strongly in the normal mode composition. For example, with S/B(FeC/FeCN) = 0.079, we calculated a ν_1 stretching frequency at 456 cm^{-1} [PED = 50% ν(FeC) and 30% δ(FeCN)] and a δ_2 bending frequency at 410 cm^{-1} [PED = 47% δ(FeCN) and 39% ν(FeC)]. With a S/B(FeC/FeCN) interaction force constant of 0.2, we calculated a 452-cm^{-1} frequency [PED = 48% δ(FeCN) and 42% ν(FeC)] and a 403-cm^{-1} frequency [PED = 47% ν(FeC) and 38% δ(FeCN)] for the δ_2 bending and ν_1 stretching motions, respectively. Thus, with a stretch–bend interaction force constant of 0.2, the latter calculation mistakenly predicts that the higher frequency results from the bending, rather than the stretching, mode. Consequently, because the former calculation agrees with the vibrational frequencies and isotopic shifts of cyanometHb CTT III (Yu et al., 1984), we used a S/B(FeC/FeCN) force constant equal to 0.079 in our force field.

Results

Vibrational Frequencies of the ν_1 Stretching and δ_2 Bending Modes. The optical spectra of MPO species are strongly red-shifted, relative to those of the corresponding HRP derivatives (Wever & Plat, 1981; Brill & Williams, 1961). Accordingly, we used 457.9 nm to achieve resonance with the Soret band of cyanoferric MPO and 413.1-nm excitation to study the axial ligand vibrations of cyanoferric HRP. Figures 1 and 2 show the low-frequency resonance Raman spectra of cyanoferric MPO and cyanoferric HRP, respectively, at pH 7.4 with several isotopically substituted cyanide species. In both cases, two isotope-sensitive lines have been identified. In MPO, the line at 361 cm^{-1} (Figure 1a) that is observed with the $^{12}C^{14}N$ isotope shifts to 359 cm^{-1} (Figure 1b,c) upon $^{13}C^{14}N$ and $^{12}C^{15}N$ substitution, respectively, and shifts further down to 356 cm^{-1} (Figure 1d) upon $^{13}C^{15}N$ substitution. Similarly, HRP shows a line at 456 cm^{-1} (Figure 2a) that shifts down to 452 cm^{-1} (Figure 2b), to 453 cm^{-1} (Figure 2c), and to 448 cm^{-1} (Figure 2d) upon $^{13}C^{14}N$, $^{12}C^{15}N$, and $^{13}C^{15}N$ substitution, respectively. Both of these vibrations, that is, the 361-cm^{-1} mode in cyano-MPO and the 456-cm^{-1} mode in cyano-HRP, show a shift toward lower energy upon an increase in the mass of the cyanide ligand. Such isotope-dependent behavior has been observed previously in cyanometHb CTT III (Yu et al., 1984; Yu & Kerr, 1988), in HbA–CO and Mb–CO (Yu et al., 1984; Tsubaki et al., 1982; Yu & Kerr, 1988), and in HRP–CO (Smulevich et al., 1986; Uno et al., 1987) and is typical of the ν_1 stretching frequency.

The second isotope-sensitive line in MPO occurs at 453 cm^{-1} (Figure 1a) for the $^{12}C^{14}N$ isotope. Its frequency shifts to 448 cm^{-1} (Figure 1b), to 453 cm^{-1} (Figure 1c), and to 448 cm^{-1} (Figure 1d) upon $^{13}C^{14}N$, $^{12}C^{15}N$, and $^{13}C^{15}N$ substitution, respectively. In HRP, the corresponding vibration is present at 405 cm^{-1} (Figure 2a) and shifts to 397 cm^{-1} (Figure 2b), to 405 cm^{-1} (Figure 2c), and to 397 cm^{-1} (Figure 2d) upon $^{13}C^{14}N$, $^{12}C^{15}N$, and $^{13}C^{15}N$ substitution, respectively. The zigzag frequency shift pattern for the 453-cm^{-1} line in MPO–CN, and for the 405-cm^{-1} line in HRP–CN upon isotopic substitution of the cyanide ligand, has also been identified in spectra of other heme iron–diatomic ligand complexes including cyanometHb CTT III (Yu et al., 1984; Yu & Kerr, 1988), HBA–CO and Mb–CO (Yu et al., 1984; Tsubaki et

Table I: Vibrational Frequencies[a] in Isotopically Substituted Cyanoferric Heme Proteins and Models

vibrational mode	isotopes			
	$^{12}C^{14}N$	$^{13}C^{14}N$	$^{12}C^{15}N$	$^{13}C^{15}N$
	HRP[b,c]			
ν_1	456	452	453	448
δ_2	405	397	405	397
	Hb[d]			
ν_1	453	450	450	446
δ_2	412	403	412	403
	MPO[c,e]			
ν_1	361 (356)	359	359	356 (352)
δ_2	453	448	453	448
	Deuteroporphyrin Dimethyl Ester[c]			
ν_1	451		446	
	Deuterochlorin Dimethyl Ester[c]			
ν_1	452		446	

[a] Vibrational frequency in cm^{-1}. [b] pH = 7.4 and pH = 10.6. [c] This work. [d] From Yu et al. (1984). [e] pH = 7.4 and pH = 10.5 (values in parentheses).

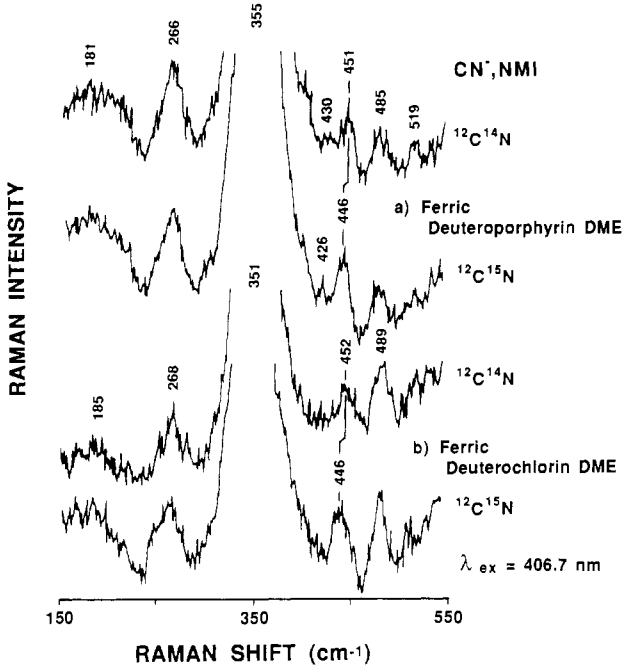

FIGURE 3: Low-frequency resonance Raman spectra of mono(1-methylimidazole), monocyanide complexes of (a) ferric deuteroporphyrin dimethyl ester and (b) ferric deuterochlorin dimethyl ester with isotopically labeled cyanide ($^{12}C^{14}N$ and $^{12}C^{15}N$). λ_{ex} = 406.7 nm; laser power 20 mW; total of three scans per spectrum.

al., 1982; Yu & Kerr, 1988), and HRP–CO (Uno et al., 1987; Smulevich et al., 1986) and is assigned to a δ_2 mode with a dominant contribution from the δ(FeCN) internal coordinate. Table I summarizes the ν_1 stretching and the δ_2 bending frequencies for isotopically substituted samples of MPO–CN, HRP–CN, and MetHb CTT III–CN.

The axial FeCN modes in MPO, relative to those in HRP and in metHb CTT III, display markedly different frequencies. This effect is sufficiently pronounced that the wavenumber magnitude of the predominantly stretching and bending modes is inverted for MPO–CN relative to HRP–CN. A possible source of this behavior is the difference in prosthetic groups that occurs in the two proteins: the active site chromophore in HRP is protoheme, whereas MPO is postulated to have an iron chlorin at its active site (Morell et al., 1967; Eglington et al., 1982; Sibbett et al., 1984; Babcock et al., 1985; Ikeda-Saito et al., 1985; Stump et al., 1987). Figure 3 shows low-frequency RR spectra for cyanoferric complexes of deuteroporphyrin dimethyl ester (Figure 3a) and deuterochlorin dimethyl ester (Figure 3b) and for their $^{12}C^{15}N$-substituted analogues. In both cases, the only band that shifts upon isotopic substitution (451 cm^{-1} in the porphyrin complex and 452 cm^{-1} in the chlorin complex) is attributed to the Fe–C stretching vibration, owing to its sensitivity to isotopic substitution at the CN^- nitrogen. Thus, the difference in macrocycle structure represented by porphyrin vs chlorin does not change the vibrations of the axial ligand–metal system, in agreement with the findings of Ozaki et al. (1986), who compared iron–ligand vibrations of octaethylchlorin complexes to those of octaethylporphyrin. Clearly, the proposed chlorin macrocycle of the MPO chromophore should not inherently perturb the iron–cyanide modes relative to those in HRP and is unlikely to be the origin of the differences apparent in Table I.

For catalytic intermediates of both HRP and MPO, the occurrence of a hydrogen-bonding amino acid residue in the ligand binding pocket has been inferred from the pH dependence of the oxoferryl stretching mode (Sitter et al., 1985;

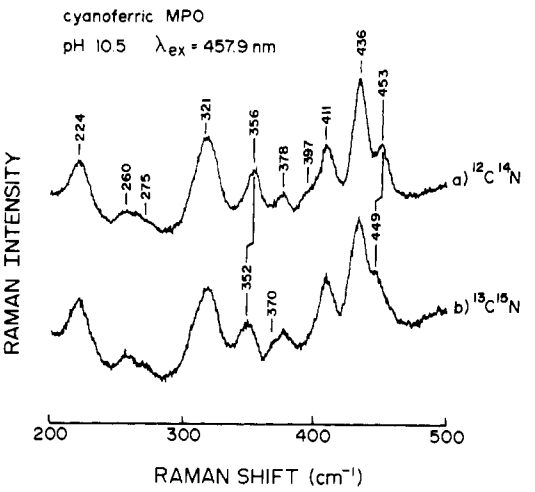

FIGURE 4: Low-frequency resonance Raman spectra of isotopically labeled cyanoferric MPO. Conditions: [enzyme chromophore] = 0.05 mM; [total cyanide] = 0.5 mM in 400 mM carbonate buffer; sample pH 10.5; λ_{ex} = 457.9 nm; laser power 40 mW; total of five to six scans per spectrum. (a) $^{12}C^{14}N$ and (b) $^{13}C^{15}N$.

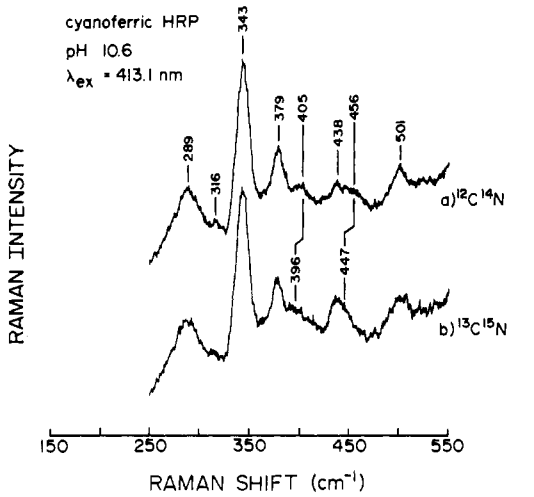

FIGURE 5: Low-frequency resonance Raman spectra of isotopically labeled cyanoferric HRP. Conditions: [enzymne chromophore] = 0.06 mM; [total cyanide] = 0.75 mM in 100 mM carbonate buffer; sample pH 10.5; λ_{ex} = 457.9 nm; laser power 30 mW; total of eight scans per spectrum. (a) $^{12}C^{14}N$ and (b) $^{13}C^{15}N$.

Table II: Effect of Decreasing the Fe–C Stretching Force Constant S(FeC) at an FeCN bond Angle of 155° on the PED of the ν_1 Stretching and δ_2 Bending Frequencies[a]

S(FeC) (mdyn/Å)	ν_1 (cm^{-1})	PED			δ_2 (cm^{-1})	PED		
		ν(FeC) (%)	δ(FeCN) (%)	ν(ImFe) (%)		ν(FeC) (%)	δ(FeCN) (%)	ν(ImFe) (%)
1.601	480	52	38	5	369	25	30	23
1.501	471	47	42	5	367	27	34	25
1.401	363	30	29	29	464	42	47	5
1.301	357	32	25	33	457	37	52	4
1.201	354	34	20	33	451	32	57	4

[a] All other force-field parameters correspond to those of metHb CTT III–CN (Table III). PED = potential energy distribution.

Hashimoto et al., 1986; Oertling et al., 1988; Oertling & Babcock, 1988). Accordingly, we have investigated the effects of pH on the FeCN modes in the cyanoferric complexes of those species. Figures 4 and 5 show the isotopic (i.e., $^{12}C^{14}N$ and $^{13}C^{15}N$, respectively) resonance Raman lines and vibrational frequencies of the ν_1 stretching and the δ_2 bending modes excited at 457.9 and 413.1 nm of cyanoferric MPO (pH 10.5) and cyanoferric HRP (pH 10.6), respectively. The vibrational frequencies of these isotopically substituted compounds are summarized in Table I. We find that, in general, the ν_1 frequency of MPO–CN decreases at the higher pH, while the δ_2 frequency does not change. In contrast, the ν_1 and δ_2 frequencies of HRP–CN do not vary over the same pH range.

Vibrational Analysis. The above results establish that the vibrational mode of predominantly ν(FeC) character occurs at a substantially lowered frequency in MPO–CN, relative to that in HRP–CN and the cyanoferric model compounds investigated. This suggests that the Fe–C stretching force constant is substantially reduced in MPO, relative to that of other complexes. Off-axis binding of the CN^- to the Fe^{3+}, to give a bent configuration in which the FeCN angle is substantially less than 180°, could reduce not only the σ bonding but also the effective π overlap between the Fe d_{xz} and d_{yz} orbitals and the CN^- π orbitals and lower the S(FeC) force constant. We employed normal coordinate analysis in order to investigate whether this bent geometry and weaker Fe–CN bond could explain the observed frequencies. The force field of our cyanoferric metalloporphyrin model system was refined to reproduce the ν_1 stretching and δ_2 bending frequencies for the natural and isotopic substitutions of metHb CTT III–CN (Yu et al., 1984), as described above. The analysis reproduces the experimental frequencies (Table I) to within 2–3 cm^{-1}. More importantly, however, the PEDs we obtained from the analysis showed that the ν_1 "stretching" and δ_2 "bending" motions are not pure modes but rather that they are each mixtures of the stretching and bending internal coordinates. Only in the case of a linear Im—Fe—C≡N geometry are the stretch and bend orthogonal; deviations from linearity produce mode mixing so that ν_1 acquires some bending character and vice versa. In this regard, our analysis is similar to those carried out for a series of hexacyano metal ions reported by Jones et al. (1971, 1974) and by Shimanouchi and Nakagawa (1972) that showed similar coupling between the ν(MC) stretching and δ(MCN) bending internal motions.

These observations provide the basis for our analysis of the reversal in frequency ordering of the stretching and bending vibrations in HRP and MPO: the extent of mixing of the two internal coordinates in the PEDs determines the ordering of the mode that is predominantly ν(FeC) in character with respect to that which is predominantly δ(FeCN) in character. The relative contributions of the stretch and the bend to the calculated normal modes is a sensitive function of the Fe–C stretching force constant, S(FeC). Figure 6 shows that, for an FeCN angle of 170°, a decrease in this force constant produces discontinuous behavior in the ν_1 stretching and the

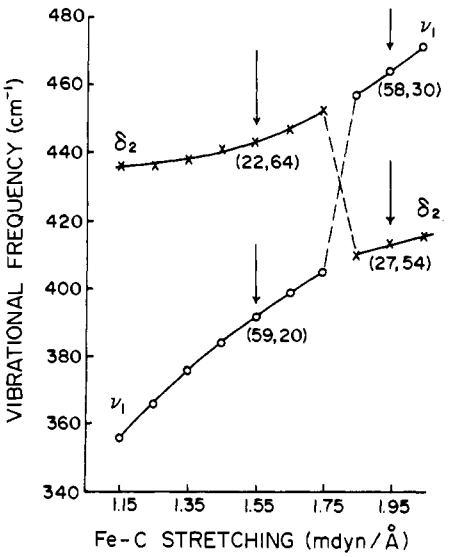

FIGURE 6: Effect of decreasing the Fe–C stretching force constant S(FeC) on the potential energy distribution (PED) and frequency (cm^{-1}) of the ν_1 and δ_2 normal modes: (○) ν_1 stretching frequency; (×) δ_2 bending frequency. (% ν(FeC), % δ(FeCN)) = PED containing the stretching and bending internal coordinate contributions, respectively. The force field used in this calculation corresponds to that of metHb CTT III–CN, given in Table III, with the exception that the Fe–C stretching force constant was varied. An angle of 170° was used.

δ_2 bending frequencies. Upon going from an Fe–C stretching force constant of 2.05 mdyn/Å to one of 1.15 mdyn/Å, a monotonic decrease is observed in both vibrational frequencies (cf. the upper and lower curves in Figure 6). Also, the PEDs for these vibrational modes change dramatically as S(FeC) decreases. For example, with an Fe–C stretching force constant equal to 1.95, the upper and lower curves indicate frequencies of 464 and 413 cm^{-1}, respectively. The PED for the higher frequency vibration has a 58% contribution from ν(FeC) and a 30% contribution from the δ(FeCN) and, correspondingly, is assigned to the ν_1 stretching mode. The lower frequency mode has a 27% ν(FeC) contribution and a 54% δ(FeCN) contribution and is assigned to the δ_2 bending mode. If the S(FeC) decreases to 1.55, then the upper and lower curves indicate frequencies of 443 and 392 cm^{-1}, respectively. However, the PED for the former frequency is 22% ν(FeC) and 64% δ(FeCN) and for the latter is 59% ν(FeC) and 20% δ(FeCN). In this case, the higher frequency must be assigned as the δ_2 bending mode and the lower frequency as the ν_1 stretching mode.

The analysis of Figure 6 indicates that a decrease in the Fe–C force constant can reverse the energy ordering of the modes in which the stretching or the bending coordinate dominates. This is represented in Figure 6 by the discontinuous lines, which, by themselves, do not represent any physical quantity but are used to indicate the region in which the reversal in ordering of the modes occurs. Figure 6, however, cannot fit quantitatively the observed MPO vibrational fre-

Table III: Optimized Force Fields[a] for Imidazole–Fe–CN[b] System in Several Cyanoferric Heme Proteins

force constant	metHb CTT III–CN	HRP–CN	MPO–CN
S(CN)	16.900	17.000	17.255
S(FeC)	1.850	1.845	1.301
S(ImFe)	1.460	1.900	1.661
S(FeN_p)	1.000	1.000	1.000
B(FeCN)	0.500	0.409	0.428
B(ImFeCN)	0.400	0.400	0.400
S/S(ImFe/CN)	0.218	0.218	0.218
S/S(FeC/CN)	0.340	0.340	0.340
S/B(FeC/FeCN)	0.079	0.079	0.079

[a] The units were mdyn/Å for the stretching (S) and stretch/stretch interaction (s/S) force constants, mdyn/rad for the stretch/bend (S/B) interaction force constants, and mdyn Å/rad^2 for the bending (B) force constants. [b] Bond lengths (Å) used were as follows: ImFe = 2.025, FeC = 1.908, CN = 1.152, and FeN = 1.970. The Im–Fe–C moiety was assumed linear and perpendicular to the porphyrin plane. The FeCN bond angle (deg) was 17 for metHb CTT III–CN and HRP–CN, respectively, and 155 for MPO–CN.

quencies. To do this, we found it necessary to vary not only the Fe–C force constant but also the FeCN bond angle. Table II illustrates the results of a similar calculation for an FeCN angle of 155°. Together, Table II and Figure 6 show that, regardless of angle, a decrease in the S(FeC) force constant decreases the ν_1 stretching frequency and increases the δ_2 bending energy. At the smaller angle, however, the ν(ImFe) stretching motion couples with the δ(FeCN) coordinate and must be included in the δ_2 PED. This fact is important in explaining the pH dependence of the MPO frequencies and the lack of such in the HRP frequencies (see below). Also, the S(FeC) value at which the frequencies invert is significantly lower (1.4 compared to 1.8 mdyne/Å) for the smaller angle. During the course of this analysis, we also studied the effects on the normal mode frequencies and PEDs of varying the FeCN angle at a constant S(FeC) value. Our results showed that decreasing the angle from 180° to 150° resulted in an increase in the ν_1 and a decrease in the δ_2 frequencies, i.e., the opposite of what we observe in the MPO–CN spectra. Thus, both the lowered Fe–C stretching force constant and the smaller FeCN angle are necessary to explain the MPO–CN results. Table III shows the optimized force field used for our final analysis. For the HRP case, we found good agreement with the experimental data for a FeCN bond angle of 170° and the following force constants: S(CN) = 17.000, S(FeC) = 1.845, S(ImFe) = 1.900, and B(FeCN) = 0.409. For the MPO frequencies, the best fit was obtained by using an FeCN bond angle of 155° and the following force constants: S(CN) = 17.255, S(FeC) = 1.301, S(ImFe) = 1.661, and B(FeCN) = 0.428. Table IV lists the optimized frequencies calculated with these parameters for both HRP–CN and MPO–CN and compares them to the experimental measurements. We found that the fit to the HRP and MPO frequencies could further be improved by small variations of B(FeCN). This accounts for the small differences in the calculated MPO frequencies in Table IV and the 155° angle results in Table II. Without the angle and S(FeC) variations, however, changes in the B(FeCN) bending force constant could not account for the MPO data.

Discussion

In cyanoferric HRP, we assign the vibrations present at 456 and 405 cm^{-1} (Figure 2) to the ν_1 stretching and δ_2 bending modes, respectively. The basis for this assignment originates in the earlier work by Yu and co-workers (Yu et al., 1984; Yu & Kerr, 1988) that showed that, upon isotopic substitution in the cyanide moiety, the frequency of the stretching coordinate decreases when the heavier isotopes of both carbon and nitrogen are used, whereas the bending coordinate is more sensitive to isotopic substitution at the carbon. Our normal coordinate analysis confirms these conclusions and emphasizes the dependence of the observed frequencies and energy ordering of the stretching and bending modes upon FeCN geometry. The cyanoferric porphyrin model compound, for which X-ray studies have shown that the FeCN moiety is linear and perpendicular to the porphyrin ring (Scheidt et al., 1980, 1983), shows an isotope-sensitive line at 451 cm^{-1} (Figure 3a). The shift observed upon isotopic substitution at the cyanide nitrogen indicates that this mode arises from the stretching vibration. The cyanoferric chlorin model compound (Figure 3b) shows similar behavior in terms of its ν_1 stretching motion. Comparison of these frequencies and structures suggests that, in HRP, the FeCN moiety adopts a geometry such that the C≡N is approximately normal to the heme plane. A similar FeCN geometry has been proposed for the cyanoferric metHb CTT III complex (Yu et al., 1984).

Aside from cyanoferric MPO, virtually all of the model heme and heme–protein complexes with CN^- examined to date display iron–ligand stretching frequencies at higher wavenumbers than the iron–ligand bending motions. The inverted wavenumber magnitude of these two vibrations in the MPO species is similar to that displayed for the metal–ligand vibrations of $Co(CN)_6^{3-}$ (Jones et al., 1971); thus, this behavior is not without precedence in transition metal–cyano complexes. Moreover, recently, Han et al. (1989) have reported a reversal in the isotopic shift patterns for the upper and lower wavenumber vibrations of an FeCN moiety in sulfite reductase. This system, however, also displays a second set of CN^- isotope-sensitive vibrational frequencies that shows the more common pattern of isotopic shifts, that is, one that is analogous to that which we observe for the HRP–CN system and that Yu et al. (1984) observed for metHb CTT III–CN. Han et al. (1989) attributed this behavior to the occurrence of different binding geometries in the heme pocket.

As discussed above, Figure 6 shows that a decrease in the Fe–C stretching force constant from 1.845 to 1.301 mdyn/Å can account for the reversed order of the ν_1 stretching and δ_2 bending energies in cyanoferric MPO. However, to calculate accurate frequencies, it was necessary to assume a bent structure with a Fe—C≡N angle of 155° rather than the

Table IV: Calculated ν_1 Stretching and δ_2 Bending Frequencies (cm^{-1}) for HRP–CN and MPO–CN

normal mode	$^{12}C^{14}N$ (Δ)[a]	$^{13}C^{14}N$ (Δ)	$^{12}C^{15}N$ (Δ)	$^{13}C^{15}N$ (Δ)	PED[b]
			HRP FeCN Bond Angle[b] = 170°		
ν_1	457 (−1)	452 (0)	454 (−1)	448 (0)	64% ν(FeC), 17% δ(FeCN)
δ_2	404 (0)	396 (1)	402 (1)	394 (3)	64% δ(FeCN), 12% ν(FeC)
			MPO FeCN Bond Angle[b] = 155°		
ν_1	359 (2)	357 (2)	357 (2)	355 (−1)	30% ν(FeC), 24% δ(FeCN), 33% ν(ImFe)
δ_2	457 (−4)	446 (−2)	455 (−2)	444 (−4)	52% δ(FeCN), 37% ν(FeC)

[a] Δ = Difference of the calculated frequencies and the experimental frequencies from Table I. [b] Potential energy distribution (PED)—total internal coordinates contribution in the calculation was 100%.

nearly linear geometry used for HRP–CN. This bent geometry has precedence in that the cyanide adduct of another closely related enzyme, cytochrome *c* peroxidase, displays an Fe—C≡N angle of 130° in the solid state (Poulos et al., 1978). Furthermore, a bent structure gives a physical basis for a decrease in the S(FeC) force constant. This decrease in S(FeC) reduces the ν_1 stretching frequency. The decrease in wavenumber of the ν_1 mode upon steric hindrance of the CN^- ligand is supported by resonance Raman studies of cyanoferric complexes of "strapped" model porphyrins (Tanaka et al., 1987). In these compounds, a hydrocarbon strap connected to opposite C_β pyrrole positions forces the CN ligand to assume distorted geometries. These authors found that, as the strap length decreases, so, too, does the ν_1 frequency. They did not observe mode reversal, however, as their compounds displayed wavenumber decreases of only 6–9 cm^{-1} for the ν_1 mode. Apparently, the geometric distortion from FeCN linearity that they were able to achieve was small.

The assignment of a bent FeCN geometry is consistent with recent work done on similar systems by Spiro and co-workers (Li et al., 1988; Han et al., 1989). The greater frequency separation between the ν_1 and δ_2 modes for MPO–CN (92 cm^{-1}) relative to that for HRP–CN (51 cm^{-1}) is consistent with bent and linear FeCN systems, respectively. That is, we find that decreasing the FeCN angle tends to mix the ν(FeC) and δ(FeCN) coordinates and drive the vibrational frequencies of the ν_1 and δ_2 normal modes apart, in agreement with the (Li et al., 1988) analysis of the FeCO system. Thus, our conclusion that a bent FeCN geometry gives rise to the reversal in frequency ordering of the ν_1 and δ_2 modes in MPO–CN agrees with the analysis of cyanoferric sulfite reductase by Han et al. (1989), as they assign two FeCN geometries for this system: a linear one giving rise to ν_1 and δ_2 frequencies of 451 and 390 cm^{-1} and a bent one yielding 352 and 451 cm^{-1}, respectively. In the notation used by these authors, our ν_1 and δ_2 correspond to their mode I and mode II, respectively.

Care must be taken, however, when the vibrational behaviors of the Fe^{3+}–CN^- and Fe^{2+}–CO systems are compared. For example, ferrous CO complexes of the same strapped porphyrins used by Tanaka et al. (1987) show trends in the ν_1 frequency opposite from those observed for the ferric CN^- complexes upon shortening the strap length (Yu et al., 1983). Furthermore, binding of CO to Fe^{2+} decreases the C=O stretching frequency, whereas binding of CN^- to Fe^{3+} increases the C≡N stretching frequency (Yoshikawa et al., 1985).

What biochemical insights can be derived from our deduction of a bent FeCN moiety in MPO vs a linear one in HRP? The cyanide binding kinetics of both HRP and MPO have been studied (Dunford et al., 1978; Bolscher, 1986). Both enzymes in the ferric state bind HCN rather than CN^-, and the rate of binding is maximal between pH 4 and pH 9. The extremes represent the pK_a's of a nearby amino acid group and of HCN, respectively. Interestingly, MPO binds cyanide faster and more tightly than does HRP (Bolscher, 1986; Ellis & Dunford, 1968), yet the Fe–C stretching force constant (hence, the bond strength) is weaker. Thus, as is the case for other Fe–ligand systems (Walters et al., 1980; Kerr et al., 1983, 1985; Masukawa et al., 1985), the free energy change that accompanies ligand binding is not localized in a single iron–ligand bond but, rather, delocalized throughout the heme pocket.

It is likely that a common feature of the peroxidase heme active site is the occurrence of both distal and proximal histidine residues (Poulos et al., 1978). The proximal residue is ligated to the iron and is thought to be hydrogen bonded

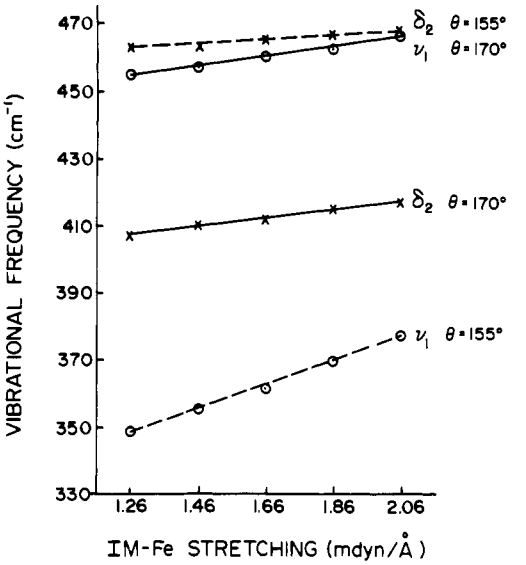

FIGURE 7: Effect of increasing the Im–Fe stretching force constant S(ImFe) on the ν_1 stretching and δ_2 bending frequencies (cm^{-1}): solid line for a FeCN geometry of 170° and discontinuous line for a FeCN geometry of 155°.

through the amino proton by another anionic residue of the pocket. This gives the proximal ligand partial anionic character that strengthens the (His)N–Fe bond relative to that of hemoglobin, as evidenced by the high ν(FeNHis) frequency of the ferrous peroxidase species (Kitagawa, 1988). The binding of HCN to the ferric enzyme is thought to involve proton transfer from the ligand to the imino nitrogen of the distal histidine. CN^- binds to the Fe^{3+} to form the cyano complex, which is hydrogen bonded through the nitrogen by the protonated distal histidine (Behere et al., 1985; Shiro & Morishima, 1986; Thanabal et al., 1988). That is, the distal configuration is Fe—C≡N···HN(His).

In cyanoferric MPO, nonlinear binding of the CN^- could be brought about by an off-axis distal hydrogen bond. This could result in a bent FeCN group. However, we could observe no difference in the ν_1 and δ_2 frequencies of samples in 70% D_2O (data not shown) from those in H_2O. Furthermore, an increase in pH above the pK_a of the distal histidine should abolish the distal hydrogen bond. Thus, if this interaction were responsible for the bent FeCN geometry, we would expect the iron–cyanide vibrations at high pH to approximate those of a linear FeCN group more closely. From Table I and Figures 1 and 4, however, we see that an increase in pH from 7.4 to 10.5 results in a decrease in the ν_1 frequency from 361 to 356 cm^{-1}, *not* an increase, as the above reasoning would predict. Thus, while the distal hydrogen bonding may well exist in MPO–CN, it is most likely not responsible for the bent FeCN geometry or for the decrease in ν_1 with increasing pH.

Rather, the pH dependence of ν_1 of MPO–CN might well result from a change in the proximal hydrogen-bonded system. Teraoka and Kitagawa (1981) demonstrated that, for the ferrous HRP system, the proximal (His)N–Fe bond was weakened upon an increase in pH above the pK_a of the distal histidine. That is, a decrease in the *proximal* ligand–iron bond strength accompanies a deprotonation of a *distal* residue. Figure 7 shows that, for a bent FeCN structure (θ = 155°), the ν_1 frequency decreases as the Im–Fe stretching force constant, S(ImFe), decreases but the δ_2 frequency does not vary. Furthermore, for a more linear FeCN structure (θ = 170°), neither frequency changes much as S(ImFe) is varied. Thus, the pH dependence of the MPO–CN frequencies—ν_1 decreases by 5 cm^{-1} whereas δ_2 does not vary at alkaline

pH—is consistent with a bent structure, while the absence of a pH effect in the HRP–CN frequencies (compare Figures 2 and 5) is consistent with a linear geometry. This reasoning further suggests that the iron–cyanide vibrational frequencies are not greatly influenced by hydrogen bonding of the cyanide nitrogen to a protonated distal residue. Furthermore, the bent FeCN structure in MPO is most likely imposed by some other, yet-unidentified aspect of the protein that results in a more constricted heme pocket than that of HRP.

In terms of function, a more constrained heme pocket for MPO than HRP is understandable. Horseradish peroxidase compound I (HRP-I) is formed by the reaction HRP + H_2O_2 $\xrightarrow{k}$ HRP-I, where $k = 1.8 \times 10^7$ M^{-1} s^{-1} (Dunford & Stillman, 1976). The rate constant for the formation of myeloperoxidase compound I (MPO-I) is 2.3×10^7 M^{-1} s^{-1} (Bolscher & Wever, 1984). Thus, in the MPO active site, the smaller area distal to the heme provides for more efficient (i.e., faster) cleavage of the HO–OH bond. This may imply that, in agreement with the mechanism proposed by Poulos and Kraut (1982), the HOOH is bound in a bent geometry and that this arrangement is more effectively achieved in MPO by the same restraints responsible for the Fe–CN geometry in the ferric enzyme. In HRP, a larger heme pocket is necessary for the approach of macrocyclic substrates (e.g., indoleacetic acid). MPO-I, however, reacts with a relatively small substrate, Cl^-, to form HOCl, a reaction that can be accommodated by a smaller heme crevice. The analogous two-electron oxidation carried out by HRP-I is of I^- for which, again, a larger area is needed.

ACKNOWLEDGMENTS

W.A.O. and G.T.B. thank Professor M. Ikeda-Saito for discussion and Dr. M. Tecklenburg for assistance in preparing the manuscript.

REFERENCES

Agner, I. (1958) *Acta Chem. Scand. 12*, 89–94.

Agner, K. (1970) in *Structure and Function of Oxidation-Reduction Enzymes* (Akeson, A., & Ehrenberg, A., Eds.) pp 329–335, Pergamon, Oxford.

Andersson, L. A., Renganathan, V., Chiu, A. A., Loehr, T. M., & Gold, M. H. (1985) *J. Biol. Chem. 260*, 6080–6087.

Andersson, L. A., Renganathan, V., Loehr, T. M., & Gold, M. H. (1987) *Biochemistry 26*, 2258–2263.

Babcock, G. T., Ingle, R. T., Oertling, W. A., Davis, J. C., Averill, B. A., Hulse, C. L., Stufkens, D. J., Bolscher, B. G. M., & Wever, R. (1985) *Biochim. Biophys. Acta 828*, 58–66.

Bakkenist, A. R. J., Wever, R., Vulsma, R., Plat, H., & van Gelder, B. F. (1978) *Biochim. Biophys. Acta 524*, 45–54.

Bakkenist, T. (1981) Ph.D. Thesis, University of Amsterdam, Amsterdam, The Netherlands.

Behere, D. V., Gonzalez-Vergara, E., & Goff, H. M. (1985) *Biochim. Biophys. Acta 832*, 319–325.

Bolscher, B. G. M. (1986) Ph.D. Thesis, University of Amsterdam, Amsterdam, The Netherlands.

Bolscher, B. G. M., & Wever, R. (1984) *Biochim. Biophys. Acta 791*, 75–81.

Brill, A. S., & Williams, R. J. P. (1961) *Biochem. J. 78*, 246–253.

Desbois, A., Mazza, G., Stetzkowski, F., & Lutz, M. (1984) *Biochim. Biophys. Acta 785*, 161–176.

Dunford, H. B. (1982) *Adv. Inorg. Biochem. 4*, 41–68.

Dunford, H. B., & Stillman, J. S. (1976) *Coord. Chem. Rev. 19*, 187–251.

Dunford, H. B., Hewson, W. D., & Steiner, H. (1978) *Can. J. Chem. 56*, 2844–2852.

Eglington, D. G., Barber, D., Thomas, A. J., Greenwood, C., & Segal, A. W. (1982) *Biochim. Biophys. Acta 703*, 187–195.

Ellis, W. D., & Dunford, H. B. (1968) *Biochemistry 7*, 2054–2062.

Han, S., Madden, J. F., Siegel, L. M., & Spiro, T. G. (1989) *Biochemistry 28*, 5477–5485.

Harrison, J. E., & Schultz, J. (1976) *J. Biol. Chem. 251*, 1371–1374.

Hashimoto, S., Tatsumo, Y., & Kitagawa, T. (1984) *Proc. Jpn. Acad., Ser. B 60*, 345–348.

Hashimoto, S., Tatsuno, Y., & Kitagawa, T. (1986) *Proc. Natl. Acad. Sci. U.S.A. 83*, 2417–2421.

Hoogland, H., van Kuilenburg, A., van Riel, C., Muijsers, A. O., & Wever, R. (1987) *Biochim. Biophys. Acta 916*, 76–82.

Ikeda-Saito, M., Argade, P. V., & Rousseau, D. L. (1985) *FEBS Lett. 184*, 52–55.

Jones, L. H., Memering, M. N., & Swanson, B. I. (1971) *J. Chem. Phys. 54*, 4666–4671.

Jones, L. H., Swanson, B. I., & Kubas, G. J. (1974) *J. Chem. Phys. 61*, 4650–4655.

Kean, R. T. (1987) Ph.D. Thesis, Michigan State University, East Lansing, MI.

Kerr, E. A., Mackin, H. C., & Yu, N.-T. (1983) *Biochemistry 22*, 4373–4379.

Kerr, E. A., Yu, N.-T., Bartnicki, D. E., & Mizukami, H. (1985) *J. Biol. Chem. 260*, 8360–8365.

Kimura, S., Yamazaki, I., & Kitagawa, T. (1981) *Biochemistry 20*, 4632–4638.

Kitagawa, T. (1988) in *Biological Applications of Raman Spectroscopy* (Spiro, T. G., Ed.) pp 97–132, Wiley, New York.

Klebanoff, S. J., & Clark, R. A. (1978) *The Neutrophil: Function and Clinical Disorders*, pp 409–488, Elsevier/North-Holland, Amsterdam.

Li, X.-Y., & Spiro, T. G. (1988) *J. Am. Chem. Soc. 110*, 6024–6033.

Makino, R., Uno, T., Nishimura, Y., Iizuka, T., Tsuboi, M., & Ishimura, Y. (1986) *J. Biol. Chem. 261*, 11110–11118.

Manthey, J., Boldt, N. J., Bocian, D. F., & Chan, S. I. (1986) *J. Biol. Chem. 261*, 6734–6741.

Matsukawa, S., Mawatari, K., Yoneyama, T., & Kitagawa, T. (1985) *J. Am. Chem. Soc. 107*, 1108–1113.

Morell, D. B., Chang, Y., & Clezy, P. S. (1967) *Biochim. Biophys. Acta 136*, 121–130.

Newton, N., Morell, D. B., Clarke, L., & Clezy, P. S. (1965) *Biochim. Biophys. Acta 96*, 476–486.

Oertling, W. A., & Babcock, G. T. (1988) *Biochemistry 27*, 3331–3338.

Oertling, W. A., Hoogland, H., Babcock, G. T., & Wever, R. (1988) *Biochemistry 27*, 5395–5400.

Ozaki, Y., Iriyama, K., Ogoshi, H., Ochiai, T., & Kitagawa, T. (1986) *J. Phys. Chem. 90*, 6113–6118.

Poulos, T. L., & Kraut, J. (1980) *J. Biol. Chem. 255*, 8199–8205.

Poulos, T. L., Freer, S. T., Alden, R. A., Xuong, N. H., Edwards, L. S., Hamlin, R. C., & Kraut, J. (1978) *J. Biol. Chem. 253*, 3730–3735.

Scheidt, W. R., Haller, K. J., & Hatano, K. (1980) *J. Am. Chem. Soc. 102*, 3017–3021.

Scheidt, W. R., Lee, Y. J., Luangdilok, W., Haller, K. J., Anzai, K., & Hatano, K. (1983) *Inorg. Chem. 22*, 1516–1522.

Schonbaum, G. R., & Lo, S. (1972) *J. Biol. Chem. 247*, 3353-3360.
Schultz, J., & Schmukler, H. W. (1964) *Biochemistry 3*, 1234-1238.
Shimanouchi, T. (1969) *Computer Programs for Normal Coordinate Treatment of Polyatomic Molecules*, Tokyo University, Tokyo, Japan.
Shimanouchi, T., & Nakagawa, I. (1972) *Annu. Rev. Phys. Chem. 23*, 217-238.
Shiro, Y., & Morishima, I. (1986) *Biochemistry 25*, 5844-5849.
Sibbett, S. S., & Hurst, J. D. (1984) *Biochemistry 23*, 3007-3013.
Sibbett, S. S., Klebanoff, S. J., & Hurst, J. K. (1985) *FEBS Lett. 189*, 271-275.
Sitter, A. J., Reczek, C. M., & Terner, J. M. (1985) *J. Biol. Chem. 260*, 7515-7522.
Smulevich, G., Evangelista-Kirkup, R., English, A., & Spiro, T. G. (1986) *J. Mol. Struct. 41*, 411-414.
Smulevich, G., Mauro, J. M., Fishel, L. A., English, A. M., Kraut, J., & Sprio, T. G. (1988) *Biochemistry 27*, 5477-5485.
Steigemann, W., & Weber, E. (1979) *J. Mol. Biol. 127*, 309-338.
Stelmaszynska, T., & Zgliczynski, J. M. (1974) *Eur. J. Biochem. 45*, 305-312.
Stump, R. F., Deanin, G. G., Oliver, J. M., & Shelnutt, J. A. (1987) *Biophys. J. 51*, 605-610.
Swanson, B. I. (1976) *Inorg. Chem. 15*, 253-259.
Swanson, B. I., & Rafalko, J. J. (1976) *Inorg. Chem. 15*, 249-253.
Tanaka, T., Yu, N.-T., & Chang, C. K. (1987) *Biophys. J. 52*, 801-805.
Terner, J., Sitter, A. J., & Reczek, C. M. (1985) *Biochim. Biophys. Acta 828*, 73-80.
Teroaka, J., & Kitagawa, T. (1981) *J. Biol. Chem. 256*, 3969-3977.
Thanabal, V., de Ropp, J. S., & La Mar, G. N. (1988) *J. Am. Chem. Soc. 110*, 3027-3035.
Tsubaki, M., Srivastava, R. B., & Yu, N.-T. (1982) *Biochemistry 21*, 1132-1140.
Uno, Y., Nishifumi, Y., Tsuboi, M., Makino, R., Iizuka, T., & Ishimura, Y. (1987) *J. Biol. Chem. 262*, 4549-4556.
Wang, J. H., Nakahara, A., & Fleisher, E. B. (1958) *J. Am. Chem. Soc. 80*, 1109-1113.
Wever, R., & Plat, H. (1981) *Biochim. Biophys. Acta 661*, 235-239.
Yoshikawa, S., O'Keeffe, D. H., & Caughey, W. S. (1985) *J. Biol. Chem. 260*, 3518-3528.
Yu, N.-T., & Kerr, E. A. (1988) in *Biological Applications of Raman Spectroscopy* (Spiro, T. G., Ed.) pp 39-95, Wiley, New York.
Yu, N.-T., Kerr, E. A., Ward, B., & Chang, C. K. (1983) *Biochemistry 22*, 4534-4540.
Yu, N.-T., Benko, B., Kerr, E. A., & Gersonde, K. (1984) *Proc. Natl. Acad. Sci. U.S.A. 81*, 5106-5110.

Glycine to Alanine Substitutions in Helices of Glyceraldehyde-3-phosphate Dehydrogenase: Effects on Stability†

Christiane Ganter and Andreas Plückthun*
Genzentrum der Universität München, Max-Planck-Institut für Biochemie, Am Klopferspitz, D-8033 Martinsried, FRG
Received February 20, 1990; Revised Manuscript Received May 22, 1990

ABSTRACT: Glyceraldehyde-3-phosphate dehydrogenase (GAPDH) from chicken was expressed in and purified from *Escherichia coli*. To investigate the physical basis of possible protein stabilization strategies, the effect of substitutions of glycine residues by alanine in helical regions was determined. One Gly to Ala substitution (G316A) located in the central core of the subunit was found to strongly stabilize the protein, while the other mutations are neutral or destabilize the protein. The effect seen for the stabilizing mutant in irreversible heat denaturation correlates with the first transition in folding equilibrium experiments that is observable by fluorescence, but not with the one detected by circular dichroism measurements or in dilution-induced dissociation experiments. The stabilizing effect of a Gly to Ala substitution therefore does not seem to be caused by an entropic effect on the unfolded state. Rather, an internal cavity is filled by the substitution G316A, probably stabilizing the native state. In large oligomeric proteins, imperfect packing may be a frequent cause of limited stability.

The resistance of proteins to denaturation is of great importance for life in extreme environments, and in biotechnology. The process of natural selection has lead to variants of many proteins that function even under extreme conditions such as high temperature, high salt, or extreme pH values (Jaenicke, 1981). Glyceraldehyde-3-phosphate dehydrogenase (GAPDH)[1] is a protein which has been adapted by nature to work under extreme conditions (Harris & Waters, 1976). Thus, it should be possible to improve the stability of variants of this enzyme upon which selective pressure has not acted.

† This work was supported by Grant BCT0372 from the Bundesministerium für Forschung und Technologie to A.P.
* To whom correspondence should be addressed.

[1] Abbreviations: GAPDH, glyceraldehyde-3-phosphate dehydrogenase (EC 1.2.1.12); EDTA, ethylenediaminetetraacetic acid; NAD, nicotinamide adenine dinucleotide, oxidized form; GAP, D-glyceraldehyde 3-phosphate.

0006-2960/90/0429-9395$02.50/0